HEFAT2014
10th International Conference on Heat Transfer, Fluid Mechanics and Thermodynamics
14 – 16 July 2014
Orlando, Florida

BENCHMARK EXPERIMENTAL DATA AND RADIATIVE HEAT TRANSFER SIMULATION

Vujičić R. M.
Heatric, Division of Meggitt
Poole, BH16 6LT
United Kingdom
E-mail: mile.vujicic@meggitt.com

ABSTRACT

This paper presents work on developing methods for analyzing radiative heat transfer between diffuse-gray surfaces using finite elements and it's experimental validation. The work was motivated by a thermal analysis of vehicle platforms. In infra-red signature prediction the thermal characteristics of an aircraft for a given flight condition, including its exhaust gas flow must be determined. A few methods for calculating face-to-face radiation such as several variations of the general named Radiosity method have been introduced in recent years. Also, a few methods based on multiple reflections have been introduced since 1960's. The method proposed in this paper presents a combination of simple Radiosity face to face method and multiple reflections and is called Multiple Reflection of View Factors (MRV) method. The method was tested on a simple testing rig. Thermo-physical properties of the samples including density, thermal conductivity, emissivity and reflectivity used in experiments were measured and presented in the paper.

The view factors were obtained using the Hemi-cube method combined with the finite element (FE) technique. Afterwards, when view factors between all elements are calculated the multiple reflections of view factors is applied.

INTRODUCTION

Thermal radiation as one of the heat transfer mechanisms is very important in many manufacturing, material processing and industrial applications. Correctly determined radiative heat transfer is a key parameter in the design process for furnaces, combustion chambers, heat exchangers, solar energy collectors etc.

One of the main goals of the aerospace industry is the development of designing tools and methods for accurate thermal analysis of aircraft structures [1].

NOMENCLATURE

N_i	[-]	Shape function
T_i	[K]	Nodal temperatures
t	[s]	Time
Q	[W]	Heat source or sink in the material
F_{ij}	[-]	View (configuration) factor between two surfaces
R	[m^{2}K/W]	Interfacial thermal resistance
T	[K]	Temperature
C_p	[W/m^{2}K]	Specific heat
k	[W/mK]	Thermal conductivity
x	[m]	Cartesian axis direction
y	[m]	Cartesian axis direction
z	[m]	Cartesian axis direction

Special characters

ε_i	[-]	Hemispherical total emissivity of surface *i*
ε_j	[-]	Hemispherical total emissivity of surface *j*
ρ_i	[-]	Hemispherical total reflectivity of surface *i*
σ	[W/m^{2}K^4]	Stefan-Boltzmann constant

FINITE ELEMENT FORMULATION

The analysis of thermal problems is well established, and there are several different approaches or techniques that can be used (finite difference, boundary element, finite element and finite volume method). The finite element method (FEM) and its application to thermal problems, where the domain is divided into small elements of various shapes and re-assembled after each element has been analyzed has become a very useful tool [2].

Using FEM the temperature is approximated in each element with some function of the form [3]:

$$T^{(e)}(x,y,z,t) = \sum_{i=1}^{r} N_i\,(x,y,z)T_i(t) \tag{1}$$

An application of the Galerkin variational procedure leads to the matrix differential equations system:

$$[M]\left\{\frac{dT}{dt}\right\} + \left[[K_C] + [K_h]\right]T = R_Q + R_q + R_h + R_r \tag{2}$$

Transient heat flow can be solved using one of several techniques such as finite difference and finite element time stepping. Results presented in this paper were obtained using an implicit (backward Euler) method as one of the finite difference time stepping methods [4]. This method is unconditionally stable for linear problems.

Radiative methods (equations) analyzed in this paper, for determining the radiative heat flux q_r, are based on the assumptions that surfaces are isothermal and the incident radiative heat fluxes on them are uniform. An average temperature of the nodes related to the surface is taken as a reference.

VIEW FACTOR CALCULATIONS

Calculation of radiative heat exchanged between any two surfaces requires determining the view (geometrical, configuration or form) factors. Several different methods (deterministic and non-deterministic) such as integration ([5], [6], [7], [8] and [9], the Monte Carlo ([10], [11], [12] and [13]) and the Hemi-cube ([14], [15] and [16]) methods have been introduced to calculate view factors in recent years. A brief description of the Hemi-cube method is given in this paper.

The Hemi-cube method

The Hemi-cube method, introduced by M. F. Cohen [14], is based on the well-known Nusselt's analogy, where the view factor is calculated using a hemisphere with a unit radius. As can be seen from **Figure 1** all patches in the environment are projected onto the hemisphere.

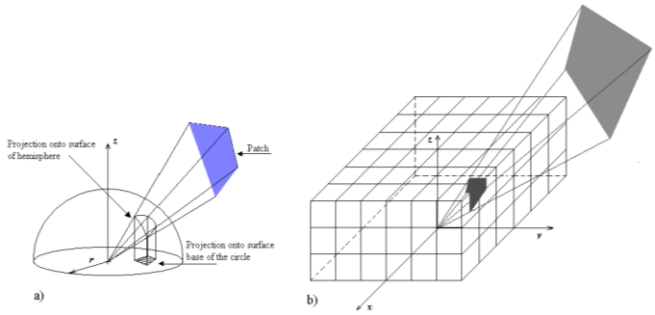

Figure 1 a) Nusselt analogy, b) the hemi-cube

The view factor is equivalent to the fraction of the circle, which is projected down onto the base of the hemisphere. Cohen's idea [14] is that it is easier to project onto an imaginary unit size hemi-cube, which is constructed around the centre of the patch, than onto a hemisphere. The hemi-cube is later divided into square 'pixels' (see **Figure 1b**).

The number of pixels depends on the chosen resolution.

Delta view factor

It should be noted that view factors are computed for each pixel. If the area of a pixel is ¢A, its view factor is:

$$\Delta View - factor = \frac{cos\phi_i\phi_j}{\pi r^2}\Delta A \qquad (3)$$

Delta view factor can be computed and stored in a look-up table.

For the top of the hemi-cube (**Figure 2a**), formula for view factor is:

$$\Delta View - factor = \frac{1}{\pi(x^2 + y^2 + 1)^2}\Delta A \qquad (4)$$

At the same time the formula for view factor calculation corresponding to the side of the hemi-cube (**Figure 2b**) is:

$$\Delta View - factor = \frac{z}{\pi(z^2 + y^2 + 1)^2}\Delta A \qquad (5)$$

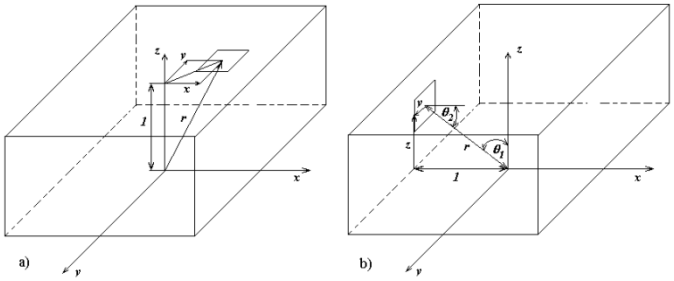

Figure 2 a) top and b) side of the hemi-cube

RADIATIVE HEAT TRANSFER SIMULATION IN NON PARTICIPATING ENVIRONMENT

According to the Stefan-Boltzmann Law the net heat exchanged between two gray surfaces A_i and A_j can be written as:

$$Q_{i\rightleftharpoons j} = \sigma\left(\varepsilon_i T_i^4 - \varepsilon_j T_j^4\right)A_i F_{i-j} \qquad (6)$$

Application of equation (6) is one of the ways to calculate the net heat exchanged between two grey surfaces. During the derivation of this equation it was assumed that surfaces act as a greybody emitter and as a blackbody receiver. Two more derivations of the flux term from Stefan-Boltzmann Law are analyzed in the text that follows.

$$Q_{i\rightleftharpoons j} = \sigma\left(\varepsilon_j T_i^4 - \varepsilon_i T_j^4\right)A_i F_{i-j} \qquad (7)$$

Equation (7) is obtained assuming that an emitter is blackbody while a receiver is greybody.

$$Q_{i\rightleftharpoons j} = \sigma\epsilon_i\varepsilon_j\left(T_i^4 - T_j^4\right)A_i F_{i-j} \qquad (8)$$

In equation (8) both emitter and receiver are greybody. Equations (6), (7) and (8) do not consider reflection. Applying simple face to face reflection which is derived from the radiosity method yields:

$$Q_{i\rightleftharpoons j} = \left[\frac{1-\varepsilon_i}{\epsilon_i A_i} + \frac{1}{A_i F_{i-j}} + \frac{1-\epsilon_j}{\epsilon_j A_j}\right]\sigma\left(T_i^4 - T_j^4\right) \qquad (9)$$

Equation (9) considers reflection between surfaces A_i and A_j without including other surfaces A_k for $k \neq i, j$.

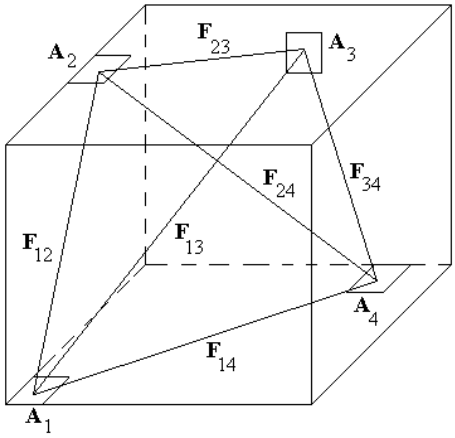

Figure 3 A general 3D enclosure

According to **Figure 3** view factor between elements 1 and 4 is 0, so we do not have any heat exchanged between them (equation (6) or equation (9)). At the same time it is obvious that some amount of the heat which leaves surface 1 will arrive onto surface 4 through reflection via surfaces 2 and 3. Seban suggested that the reflectivity could be expressed as the sum of a diffuse and a specular component. Based on this idea firstly Mahan and Eskin introduced the concept of the *radiation distribution factor*, then later Mahan [18] defined the *total radiation distribution factor* as the fraction of the total radiation emitted from a surface element *i* that is absorbed by a surface element *j*, due both to direct radiation and all possible reflections within the enclosure. This definition includes directional emission and absorption and bidirectional reflection.

THE MULTIPLE REFLECTION OF VIEW FACTORS (MRV) METHOD

One of methods to include reflectivity is the Monte Carlo Ray Tracing Method, where a ray is shot from area 1, then after reflection from area 2, arrives onto area 3. Due to reflection at area 2 the amount of energy carried by this ray is decreased for the amount of energy absorbed by area 2. This is a very time consuming method, so to shorten CPU time the MRV method is proposed. The main idea behind the MRV method is that instead tracing a ray the MRV method traces the view factor between surfaces (areas).

The basic idea of the MRV method can be explained using **Figure 3**. **Figure 3** considers four elements defined with their own total hemispherical emissivity and total hemispherical reflectivity, with view factors $F_{1\text{-}2}$; $F_{1\text{-}3}$; $F_{2\text{-}3}$; $F_{2\text{-}4}$ and $F_{3\text{-}4}$ between them.

The net heat exchanged between elements is given in the following expressions:

$$Q_{1\text{-}2} = f^n(F_{1\text{-}2})$$
$$Q_{1\text{-}3} = f^n(F_{1\text{-}3})$$
$$Q_{2\text{-}3} = f^n(F_{2\text{-}3})$$
$$Q_{2\text{-}4} = f^n(F_{2\text{-}4})$$
$$Q_{3\text{-}4} = f^n(F_{3\text{-}4})$$

$\alpha_2 Q_{1\text{-}2} = \alpha_2 f^n(F_{1\text{-}2})$ is absorbed heat by element 2, while $\rho_2 Q_{1\text{-}2} = \rho_2 f^n(F_{1\text{-}2})$ is heat reflected to the surroundings. According to the MRV method $\rho_2 f^n(F_{1\text{-}2})F_{2\text{-}3}$ is heat reflected from element 2 that arrives to element 3, while $\rho_2 f^n(F_{1\text{-}2})F_{2\text{-}4}$ is heat that arrives to element 4. After reflection the view factor is reassembled.

For example the view factor $F_{1\text{-}3}$ between surfaces 1 and 3 is reassembled into

$F_{1\text{-}3} = F_{1\text{-}3direct} + F_{1\text{-}3ref\text{-}2} + F_{1\text{-}3ref\text{-}2ref\text{-}4}$.

Obviously, calculation of all these reflections must stop at some stage. The criterion used in the MRV method is given in the following expression:

$$\frac{\left(F_{i-j}F_{j-k}F_{k-l}\rho(j)\rho(k)\cdot 100\right)}{F_{i-j}} \leq 0.1 \qquad (10)$$

With this criteria, the calculations will stop if satisfied (if heat received at element *l* from the initial element *i* is less or equal to 0.1 per cent of heat exchanged between element *i* and element *j* which is the second in the chain). View factor values are reassembled (reflectivity added to the old value) and applied to equation (9). To satisfy the conservation of energy the whole domain is surrounded by a large environmental box. View factors between each element and the environmental box are also calculated.

EXPERIMENTAL DATA

A simple testing rig which allows experiments to be performed that combine view factor effects with measured heat transfer was built, according to an original design [21]. It consists of a track (which is contained within a heat resistant low reflectivity painted box), supporting both an emitter and a receiver of various shapes, sizes and constitutive materials.

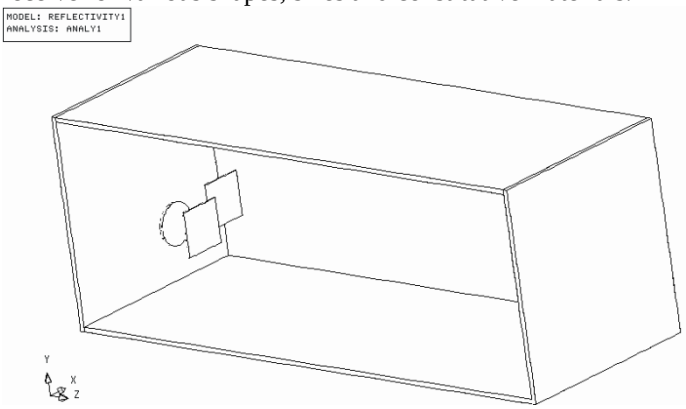

Figure 4 3D enclosure (testing rig)

The experimental work used three emitters: a black painted cylinder (made of brass) of dimensions ϕ28x197 [mm], a disc (made of steel) of diameter D = 182 [mm] and a square shaped emitter (made of steel) of dimensions 197x197 [mm]. The receiver had dimensions of 197x197 [mm] and was composed of steel, brass or aluminium, with thicknesses ranging from 3 to 15 [mm]. Also, the receiver and the emitter were able to rotated to sustain angles ranging from 0 to 360 [°] between them. The distance between the emitter and the receiver could be varied from 0 to 4 (dimensionless c=D).

In this paper only one case is presented, in which the disc is used as emitter, with two receivers; receiver 1 composed of brass with the thickness of 7 [mm] and receiver 2 composed of aluminium with same thickness (**Figure 5**), while more detailed benchmark data has been published in [22].

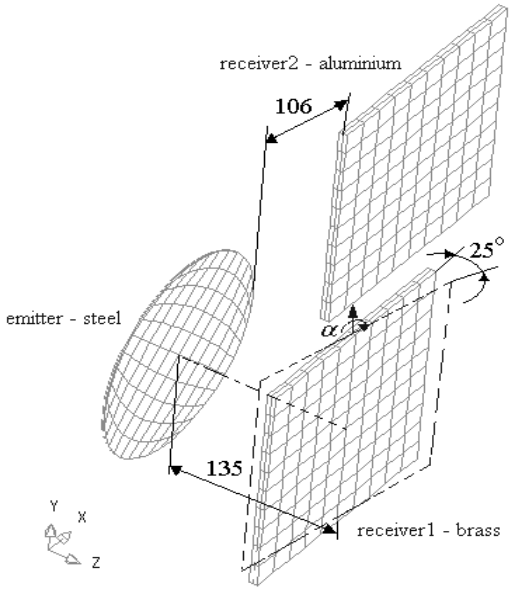

Figure 5 Detail of an emitter and receivers

Thermophysical properties of materials

Thermal conductivity of materials used in experiments was measured using an instrument called the HT11 from the "Armfield" company. To find the thermal conductivity of plates used as receivers in the experiments, three discs with of a 25 [mm] diameter were cut. Using this instrument measurements were then taken three times for each specimen using different heat fluxes, (a result of different voltages 10, 15 and 20 [V]). The thermal conductivities measured for the samples are given in **Table 1**. Thermophysical properties were assumed to be constant with temperature.

	material	**den.[kg/m^3]**	**C_p[J/kgK]**	**k[W/mK]**
Emit.(1.1)	steel	8030	503	18.9
Emit.(1.2)	ceramic	1600	800	0.1
Rec. 1	brass	8714	385	124.5
Rec. 2	alum.	2700	963	232.7
box	wood	1600	840	0.69

Table 1 thermophysical properties

Surface properties of samples used in these experiments were obtained using SOC-100 Hemispherical Directional Reflectometer. The SOC-100 Hemispherical Directional Reflectometer provides polarized, angular reflectivity measurements from 10 to 80 incident angles. Coupled to the Nicolet Magna (tm) FTIR, the SOC-100 works in the entire spectral region available for that FTIR. It has the capability to measure the collimated and scattered transmittance of samples, and by using a specular beam blocker, the diffuse and specular partition of the scattered energy. From the direct measurements other values can be calculated directional and near normal emissivity, directional angular emissivity, total hemispherical emissivity, solar absorptivity, and optical constants. Hemispherical emissivity (HE) values of the materials used in experiments, for wavelengths in the region from 2 [μm] to 25 [μm], are presented in **Figure 6**.

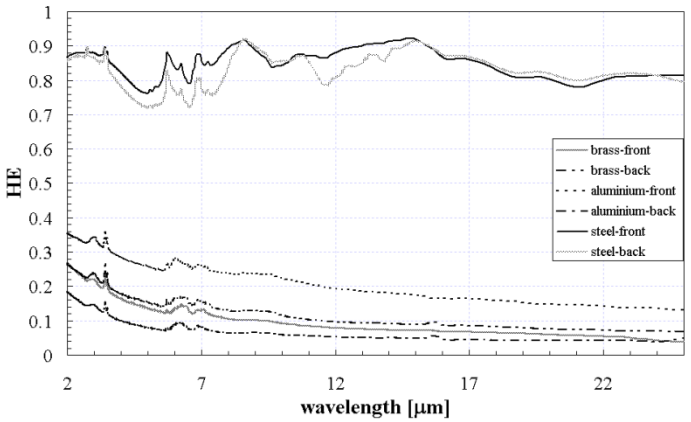

Figure 6 Hemispherical emissivity of samples

This wavelength region in thermal radiation is the near infrared. From **Figure 6** the front side of the black painted steel sample is noted as steel-front. The back side of the black painted steel sample is noted as steel-back. It can be seen that, except at short wavelengths, the difference between hemispherical emissivity trends taken from the front and back sides of the black painted steel sample are almost negligible. Also, in **Figure 6** the front side of the sample composed of brass is noted as brass-front, and the back side is noted as brass-back. The front side of the sample composed of aluminium is noted as aluminium-front, and the back side of the same sample is aluminium-back.

Directional hemispherical reflectance (DHR) for an angle of incidence of 8 [°] for wavelength region from 0.3 [μm] to 2.5 [μm] is presented in **Figure 7**. This wavelength region in thermal radiation goes from the ultraviolet to the near infrared region.

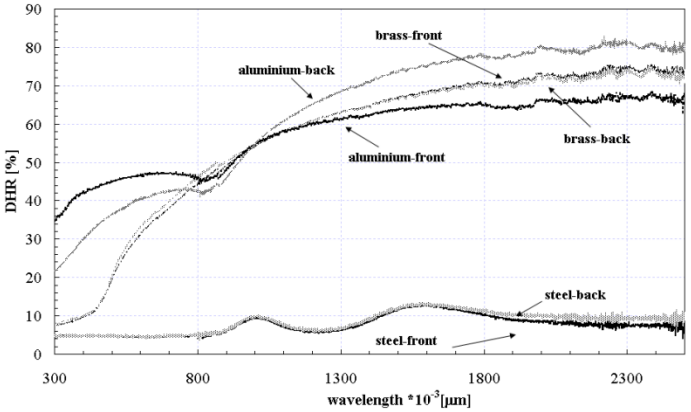

Figure 7 Directional hemispherical reflectivity of samples

Calibration and error analysis

For temperature measurement K-type thermocouples were chosen. Unfortunately, during the calibration of data logger an error between the real and the read temperature was noticed. The following diagram (**Figure 8**) presents the error for the thermocouple No. 1. As can be seen from this diagram the error has a polynomial progression and depends on the temperature.

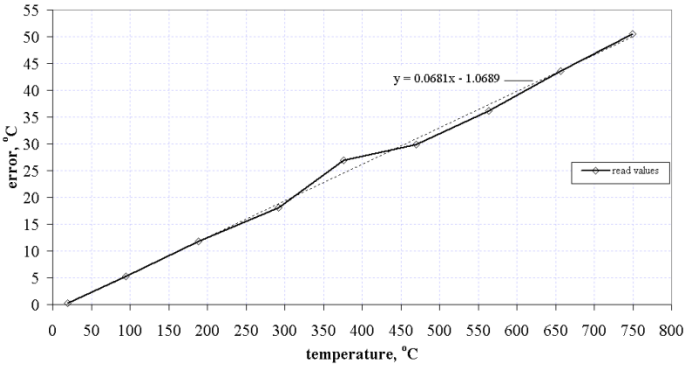

Figure 8 Total error during measurement

The difference between the real and the calibration temperature called total error ((t_{read}-t_{cal}) x 100/t_{read}) is the largest for temperature about 380 [°C], and it is less than 2 [°C] (i.e. less than 0.7%). For other operating temperature regions this error is less than 0.1 %.

Experimental data presented in **Table 2** considers four different cases (**see Figure 5**):

Case 1 - the emitter and receiver 2 (receiver 2 composed of aluminium has emissivity and reflectivity as presented in **Figures 6** and **7**) are co-planar and parallel to the receiver 1;

Case 2 - the emitter and receiver 2 (receiver 2 composed of aluminium is painted black and emissivity and reflectivity of values were used as taken from black painted steel presented in **Figures 6** and **7**) are co-planar and parallel to the receiver 1;

Case 3 - the emitter and receiver 2 (receiver 2 composed of aluminium with emissivity and reflectivity as presented in **Figures 6** and **7**) are co-planar and receiver1 is angled at 25 [°] with respect to their plane; and

Case 4 - the emitter and receiver 2 (receiver 2 composed of aluminium with black paint and with emissivity and reflectivity as from black painted steel presented in **Figures 6** and **7**) are co-planar and receiver1 is angled at 25 [°] with respect to their common plane.

Temp [K]	Case 1	Case 2	Case 3	Case 4
t_{brass1}	323.81	315.92	314.42	312.284
T_{brass2}	323.91	316.02	315.49	313.457
T_{brass3}	324.36	316.67	315.38	313.14
T_{brass4}	325	317.15	316.15	314.15
T_{Al1}	297.61	298.11	299.45	302.35
T_{Al2}	297.62	298.11	299.45	302.65
T_{Al3}	297.43	297.57	298.92	302.13
T_{Al4}	297.85	297.36	298.92	301.92
T_{e1}	717.31	707.9	703.09	703.41
T_{e2}	730.15	723.15	720.15	718.15
T_{amb}	292.95	291.15	291.65	289.95

Table 2 Temperatures of emitter, receivers and ambient for different test cases

Two thermal images presented in **Figures 9** and **10** show temperature distribution of the box mainly as result of reflection from the receiver 1. Also, receiver 2 was warmed up by reflection from receiver 1. To give a more detailed presentation three line profiles are given in **Figure 9**, while ten random points were chosen in **Figure 10**.

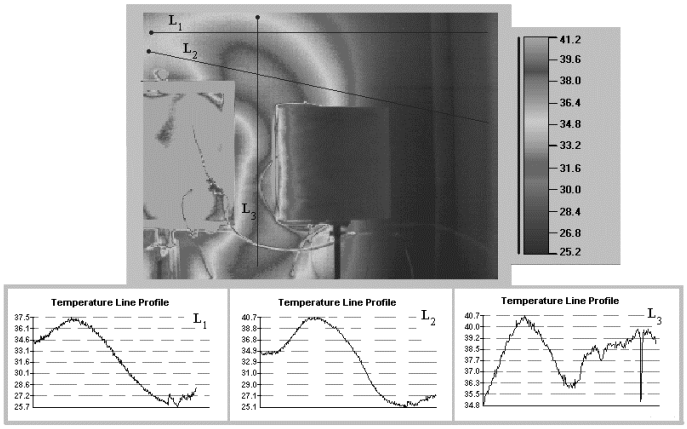

Figure 9 Temperature distribution of the box behind the emitter

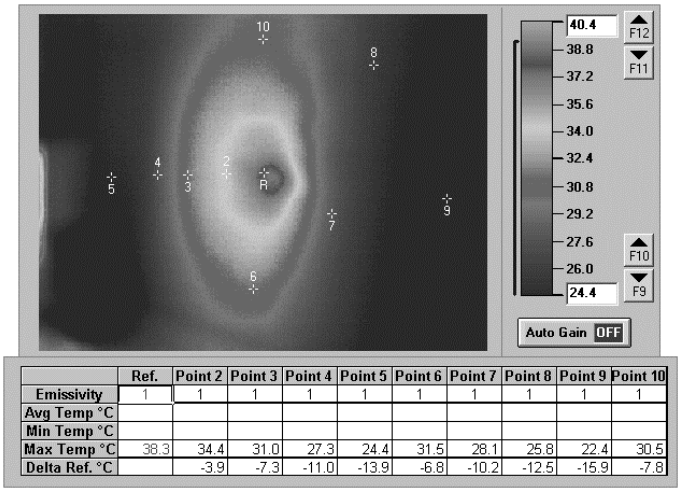

	Ref.	Point 2	Point 3	Point 4	Point 5	Point 6	Point 7	Point 8	Point 9	Point 10
Emissivity	1	1	1	1	1	1	1	1	1	1
Avg Temp °C										
Min Temp °C										
Max Temp °C	38.3	34.4	31.0	27.3	24.4	31.5	28.1	25.8	22.4	30.5
Delta Ref. °C		-3.9	-7.3	-11.0	-13.9	-6.8	-10.2	-12.5	-15.9	-7.8

Figure 10 Temperature distribution of the box exposed to reflection of receiver 1 and receiver 2

HEAT TRANSFER SIMULATION AND DISCUSSION

Results obtained for case 1 where all three modifications of the Stefan-Boltzmann Law, simple face to face radiosity ([23]) and the MRV method will be presented in this section.

For this case the domain was discretized by the following mesh resolutions using eight noded hexahedral finite elements:

a) emitter (steel layer - 10x10x2=200 elements,
insulation layer - 10x10x5=500 elements),
b) receiver 1 - 10x10x4=400 elements,
c) receiver 2 - 10x10x4=400 elements, and
d) boundary box - 3200 elements in total.

The temperature distribution of the internal side of the boundary box using face to face radiosity method, where 30,000 rays were used for the view factor calculation, is presented in **Figure 11**. This figure shows hot spots which were noticed earlier during the experiments (see **Figure 9**).

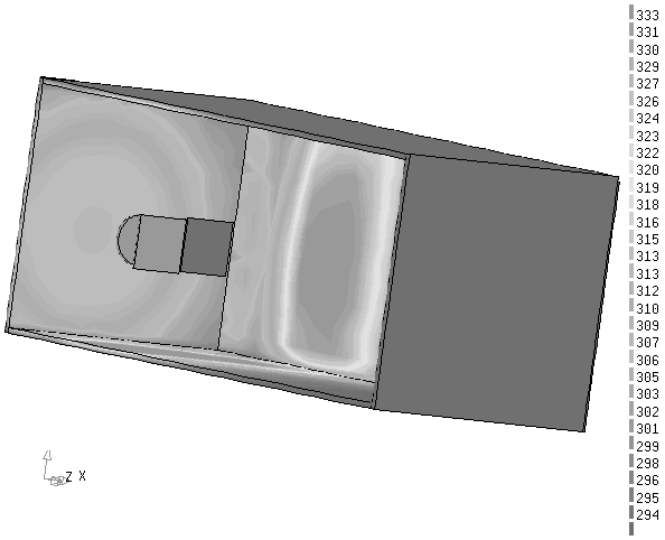

Figure 11 Temperatures of the enclosure using 30,000 rays per element (eq(9))

A comparison between **Figure 11** and **Figure 9** shows that there is a good agreement between the calculations and the experimental data (thermal image camera). Radiative flux exchanged within the enclosure is presented in **Figure 12**.

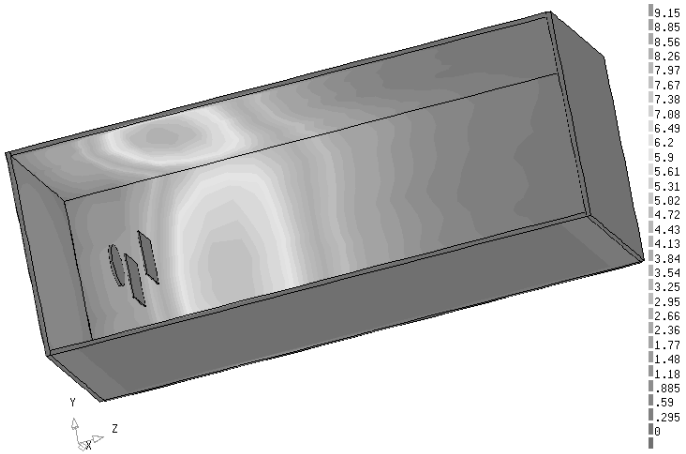

Figure 12 Radiative flux exchanged in enclosure using 30,000 rays per element (eq(9))

Further analysis which includes a comparison between the numerical results obtained using the MRV method, presented in **Figure 13**, and experimental data, presented in **Figure 9**, shows there is excellent agreement between them.

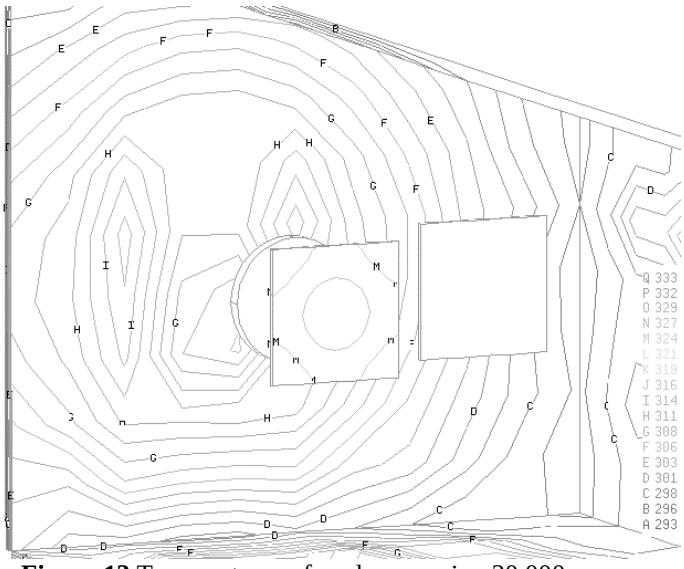

Figure 13 Temperatures of enclosure using 30,000 rays per element and the MRV method

As can be seen from **Figure 9** the peak temperature of the internal side of the box was measured at 313.85 [K], while the calculated temperature was 314 [K]. The difference between experimental and numerical results, calculated as $(t_{exp}-t_{num})$ x $100/t_{num}$, in this particular case was less than 0.05 %. Also, it can be noted in Figure 13 that minimal temperatures of temperature line profile $L1$ and $L2$ were 298.9 [K] and 298.25 [K] respectively. The temperature obtained for this region using the MRV method was just above 298 [K]. There is therefore excellent agreement between the numerical results and experimental data.

The average transient temperatures of the emitter and receivers obtained using the MRV method are presented in **Figure 14**.

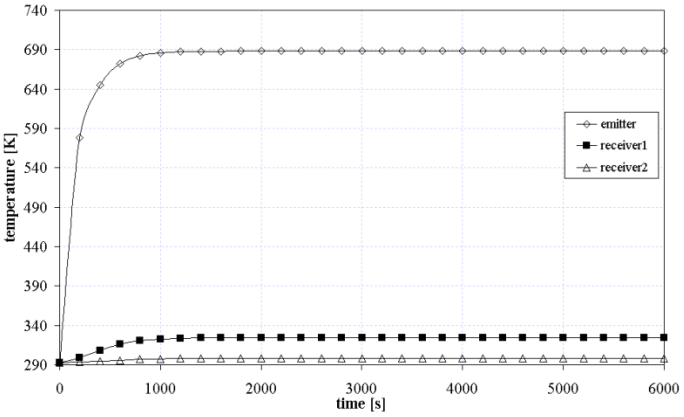

Figure 14 Average transient temperatures of the emitter and receivers using MRV method

Further analysis which includes a comparison between methods included in this paper, where average temperatures of receiver 2 (numerical and experimental) were taken as criteria (**Figure 15**), shows the advantage of the MRV method over the other methods.

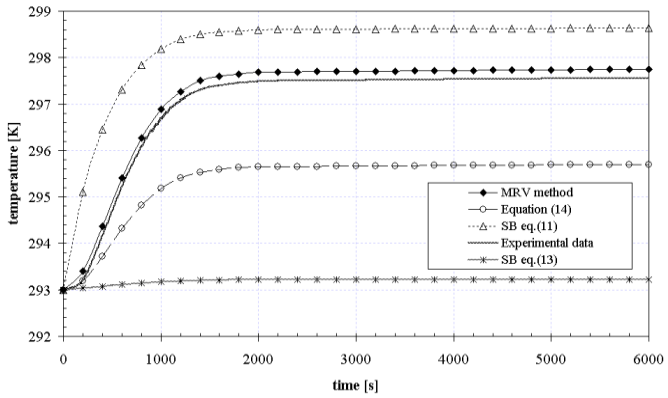

Figure 15 Average transient temperatures of receiver 2

The temperature at the centre of the emitter, and the average temperatures of receivers and boundary box with experimental data using all three variations of the Stefan-Boltzmann Law, face to face radiosity and MRV method are given in **Table 3**.

Temp [K]	Exp.	Eq(6)	Eq(7)	Eq(8)	Eq(9)	MRV
emitter	723.73	736	736	753	719.3	723.8
Rec. 1	324.27	316.9	300.44	302.6	324.02	324.312
Rec. 2	297.56	298.64	293.05	293.22	295.7	297.74
box		293.1	293.1	293.0	295.8	296.1
Amb.	292.9					

Table 3 Average temperatures of bodies in enclosure using different methods

In **Table 3** can be seen that the MRV method gives the most accurate results.

Obviously, the accuracy of the results obtained highly depends on the accuracy of the view factor values [24]. This is the main reason for using 30,000 rays per element. The difference between numerical results and experimental data is within 0.013% (using Celsius temperature scale the difference is 0.08 %) for the emitter and receiver 1. Difference between the average temperature of the receiver 2 obtained using MRV method and the measured temperature was about 0.11% (using Celsius temperature scale the difference is 1.4 %). Difference between the average temperatures obtained using face to face radiosity method and experimental data was from 0.6% (0.49 %) to 1.03% (12.7 %). All three standard variations of the Stefan-Boltzmann Law have been found to be the least accurate.

CONCLUSION

Several different methods for the radiative heat transfer simulation were presented in this paper. In particular, the Hemi-cube method, used as the ray-tracing method to calculate view factors, is also described.

The Multiple Refection of View Factors (MRV) method as proposed in this paper, has the potential to provide a better design tool which can be used in radiative heat transfer calculations.

A minimization of the error as a result of the assumptions introduced in Finite Element Formulation requires that the mesh size has to be controlled to limit the temperature variation over an element. When large temperature variations throughout structures are involved this can lead to a large number of elements. An increase in the number of elements is followed by an increase in the CPU time required for the view factor calculations. The MRV method requires a further increase in the CPU time prior to the thermal analysis, which is it's primary disadvantage. This problem could be reduced via application of parallel techniques, for which the MRV method as well as the ray tracing methods (the Monte Carlo and the Hemi-cube methods) for view factor calculation are highly suitable. A parallelization that can be used to obtain an approximately linear speed up in radiative heat transfer applications, with respect to the number of processor used.

REFERENCES

[1] Aeronautics and Space Transportation Technology, Three Pillars for Success, *National Aeronautics and Space Administration*, 1997.
[2] Smith IM and Griffiths DV, *Programming-The Finite Element Method, John Willey and Sons*, 1998.
[3] Lewis RW, Morgan K, Thomas HR, and Seetharamu KN, *The Finite Element Method in Heat Transfer Analysis, John Willey and Sons*, 1996.
[4] Vujičić MR, Finite Element Solution of Transient Heat Conduction Using Iterative Solvers. *Journal of Engineering Computations*, 23(4):408-431, 2006.
[5] Sparrow EM, A New and Simpler Formulation for Radiative Angle Factors, *Journal of Heat Transfer*, pages 81-87, May 1963.
[6] Mitalas GP and Stephenson DG, Fortran iv programs to calculate radiant interchange factors, *Technical report*, 1966.
[7] Minning CP, Calculation of shape factors between rings and inverted cones sharing a common axis, *Journal of Heat Transfer*, 99:492-494, August 1977.
[8] Juul NH, View factors in radiation between two parallel oriented cylinders of finite length, *Journal of Heat Transfer*, 104:384-388, May 1982.
[9] Shapiro AB, Facet-A radiation view factor computer code for axisymmetric, 2D planar, and 3D geometries with shadowing, *Technical report*, 1983.
[10] Ballance JO and Donovan J, Radiation configuration factors for annular rings and hemispherical sectors. *Journal of Heat Transfer*, 95:275-276, May 1973.
[11] Howell JR, The Monte Carlo method in radiative heat transfer. *Journal of Heat Transfer*, 120:547-560, 1998.
[12] Farmer JT and Howell JR, Comparison of Monte Carlo Strategies for Radiative Transfer in Participating Media, *Advances in Heat Transfer*, 31, 1998.
[13] Baranoski GVG, Rokne JG, and Guangwu X, Applying the exponential Chebyshev inequality to the nondeterministic computation of form factors, *Journal of Quantitative Stectroscopy and Radiative Transfer*, 69:447-467, 2001.
[14] Cohen MF and Greenberg DP, The Hemicube: A radiosity solution for complex enviroment. *Computer Graphics(SIGGRAPH 85)*, pages 31-40, 1985.
[15] Nishita T and Nakamae E, Continuous Tone Representation of Three-Dimensional Objects Account of Shadows and Inter reflection, *Computer Graphics (SIGGRAPH 85)*, pages 23-27, 1985.
[16] Emery AF, Johansson O, Lobo M, and Abrous A. A, comparative study of methods for computing the di®use radiation view factors for complex structures. *Journal of Heat Transfer*, 113:413-422, May 1991.
[17] Vujičić MR, Lavery NP, and Brown SGR, Benchmark Experimental Data for Radiative Heat Transfer Prediction, *3rd MIT Conference on Computational Fluid and Solid Mechanics*, pages 932-935, Cambridge, 2005, Massachusetts Institute of Technology.

[18] Mahan JR, *Radiation Heat Transfer: A Statistical Approach, John Wiley& Sons* Inc., 2002.
[19] Gebhart B, Surface temperature calculations in radiant surroundings of arbitrary complexity - for gray, diffuse radiation, *International Journal of Heat and Mass Transfer*, 3:341-346, 1961.
[20] Siegel R and Howell J, *Thermal Radiation Heat Transfer*, *Taylor and Francis*, 2002.
[21] Vujičić MR, Lavery NP, and Brown SGR, Thermal Benchmark Experimentation Data for Numerical Simulation of Radiative Heat Transfer, *8th UK Heat Transfer Conference*, Oxford, 2003, University of Oxford.
[22] Vujičić MR, Lavery NP, and Brown SGR, New Experimental Data for the Validation of Radiative Heat Transfer, *Experimental Heat Transfer*, 19(3):193-207, 2006.
[23] Vujičić MR, Lavery NP, and Brown SGR, View Factor Calculation Using Monte Carlo Method and Experimental Validation in Radiative Heat Transfer, *9th National UK Heat Transfer Conference*, Manchester, 2005, UMIST.
[24] Vujičić MR, Lavery NP, and Brown SGR, View Factor Calculation Using the Monte Carlo Method and Numerical sensitivity, *Communications in Numerical Methods in Engineering*, 22(3):197-203, 2006.